[AMERICAN JOURNAL OF SCIENCE, VOL. 295, MARCH, 1995, P. 282–308]

SOURCE OF CARBONATE AND ORIGIN OF ZONATION IN PYRITIFEROUS CARBONATE CONCRETIONS: EVALUATION OF A DYNAMIC MODEL

MAX L. COLEMAN* and ROB RAISWELL**

ABSTRACT. Spheroidal, diagenetic concretions in the Toarcian black shales of the Jet Rock (Yorkshire, United Kingdom) are predominantly calcite with a microspar texture. Pyrite occurs within the concretions, but its concentration increases to the margins to form a sharply-defined massive pyrite rim. This striking zonation can be described by a dynamic model with the following characteristics.

In an initial, pre-concretionary stage, framboidal pyrite resulted from pervasive sulfate reduction in porewaters containing dissolved iron (produced by local iron-reduction), but diffusive loss of the alkalinity generated to overlying seawater precluded carbonate precipitation. Subsequently, conditions for concretionary carbonate precipitation were created by localized sulfate reduction which caused direct precipitation of euhedral pyrite from surrounding pore-fluids with lower concentrations of reduced iron. During concretion growth the rate of generation of sulfide in the core of the concretion exceeded the rate of inward diffusion of reduced iron. The resultant centrifugal diffusion of sulfide allowed precipitation of carbonate and defined the growth zone for euhedral pyrite, which formed the rim.

Thus, the mineral zonation of the concretions was spatially rather than temporally controlled, and successive zones do not represent changes in porewater composition during burial. The model is consistent with observations of the chemical and isotopic compositions, size, shape, and stratigraphic distribution of concretions. However, the model requires very specific porewater environments not found in present-day sediments and relies on reactions that have not been described in specific detail.

INTRODUCTION

Spheroidal carbonate concretions are a common product of diagenesis in organic carbon-bearing sediments. In the (Toarcian) Jet Rock, stratigraphically localized beds of carbonate concretions are particularly well-exposed on a wave-cut platform due to differential weathering of the surrounding, less well-cemented shale. These concretions are also of interest because of their distinctive pyritiferous margins.

Previous investigations of these concretions (Raiswell, 1976, 1982; Coleman and Raiswell, 1981) have led to a model attributing their growth in well-defined beds to the existence of a thin zone of enhanced carbonate supersaturation, stabilized at a fixed distance below the sediment-water interface by a pause in deposition (Raiswell, 1987). However, although this equilibrium model was able to utilize stable isotope and geochemical data to identify the role of microbiological sulfate reduction as a source of

* Postgraduate Research Institute for Sedimentology, The University, Reading RG6 2AB, United Kingdom and BP Exploration, Chertsey Rd, Sunbury-on-Thames, Middlesex TW16 7LN, United Kingdom.

** Department of Earth Sciences, The University, Leeds LS2 9JT, United Kingdom.

the dissolved carbonate and of sulfide for concretionary calcite and pyrite growth, it is unable to identify the factors that controlled the siting and distribution of the concretions and their mineral zonation.

This paper will re-examine the isotopic, geochemical, and sedimentological constraints on the origins of the Jet Rock carbonate concretions. Data will be drawn substantially from the Jet Rock concretions, but the discussion will be generally relevant to other carbonate concretions. An alternative dynamic model will be presented which semi-quantitatively reconciles the chemical and isotopic compositions of such concretions with the spatial distributions of the components and their textures. It will be shown that this model provides a more satisfactory explanation of some features of the concretions, especially their pyrite zonations, than the alternative equilibrium model.

SAMPLE DESCRIPTIONS

Concretions occur in sediments of the Falciferum zone of the Upper Lias, Lower Jurassic (the Jet Rock) exposed on the northeast coast of Yorkshire (England). At Port Mulgrave, 11 km northwest of Whitby, the Jet Rock consists of fine-grained, well-laminated organic-rich shales in which four main concretionary horizons have been identified. These horizons have been described and numbered by Howarth (1962).

A concretion was chosen from each of two horizons: concretion UA came from bed 33 (the Cannonball Doggers) and concretion UB from bed 37 (the Curling Stones). The Cannonball Doggers range from flattened elongate bodies to regular ellipsoids (30 cm max diam), whereas the Curling Stones are larger (70 cm max diam) and are commonly oblate spheroids. In each case the host sediment is differentially compacted around the concretion. This demonstrates that the concretion grew and was cemented in relatively uncompacted sediment. It was because of the morphological evidence for an early origin that these concretions were originally chosen for geochemical analysis (Raiswell, 1976).

Petrography

In thin section the host sediments are finely-laminated bituminous shales containing abundant pyrite framboids (< 20 μm diam) in a matrix consisting of fine-grained clay and organic material with some silt-sized quartz grains. Some aragonitic fossil debris still exists, but many of the ammonites are preserved as pyrite, their aragonitic shells having been dissolved. Macroscopically, pyrite is also present in a variety of crystal forms, mainly as cubes and as hopper-shaped octahedra (Carstens, 1986).

The carbonate cement in the concretion has a microsparite texture within which shell material floats (and is more abundant than in the surrounding sediments). Pyrite is also present throughout the concretion from center to margin but becomes progressively more abundant toward the margin (Raiswell, 1976). The pyrite inside the concretion has two texturally and isotopically distinct forms (Coleman and Raiswell 1981;

Raiswell, 1982). An early framboidal phase is essentially identical with that in the host sediment and, within the concretion, is overgrown by a coarser, euhedral pyrite. There is no textural evidence to suggest that the euhedral pyrite grew by dissolution and replacement of carbonate.

Sampling Pattern

Concretions were prepared for analysis as described initially in Raiswell (1976). Each concretion was cut open, and a slice removed from its center, parallel to the bedding plane. This slice was further subdivided successively from the center outward into a series of samples lying in concentric zones (identified by i, ii, et cetera). All the concentric zones, except the central one, contain four different samples. This sampling scheme and the samples themselves are those used by Raiswell (1976) and Coleman and Raiswell (1981), who showed that the concretions exhibited radially symmetric chemical and isotopic variations. Thus, the data discussed here are from a representative edge-center-edge traverse for which both chemical and isotopic data are available.

METHODOLOGY AND RESULTS

Data for the carbonate and sulfide contents of each sample are taken from Raiswell (1976). Carbonate contents were determined by solution in 0.5 m acetic acid followed by analysis for cations by atomic absorption (Ca, Mg, Sr, Mn) and colorimetry (Fe). Summing these analyses and their carbonate equivalents gave the total carbonate content of each sample. Sulfide sulfur was measured gravimetrically following the procedure of Maxwell (1968, p. 483).

Isotopic data for the concretionary carbonates were reported by Coleman and Raiswell (1981). Samples were treated with a 1 percent cold solution of sodium hypochlorite to destroy organic matter, then washed, and dried. Carbon dioxide was liberated by reaction with 100 percent phosphoric acid (McCrea, 1950) and analyzed isotopically using a Micromass 602-C mass spectrometer.

Relevant data are presented in table 1 in the usual notation, where the isotopic compositions are presented as permil (‰) variations with respect to PDB ($\delta^{13}C$) and Canyon Diablo Troilite ($\delta^{34}S$).

All data have been corrected for instrumental and isotopic effects (Coleman and Raiswell, 1981). Carbonate and sulfide contents are expressed as calcium carbonate and pyrite respectively, in accordance with the observed mineralogy.

GENETIC MODELS

Features to be Accommodated In a Genetic Model

In summary, any model of concretionary growth is constrained by the following observations

1. *Shape.*—The concretions are spheroidal.

2. *Concretionary horizons.*—Concretions are concentrated in a few well-defined horizons.

TABLE 1

Mineralogical and isotopic compositions of the Jet Rock concretions

Sample No.	*Zone No.*	*Mineralogical Composition* (wt percent) Calcite	Pyrite	*Isotopic composition, permil* $\delta^{13}C_{PDB}$ $CaCO_3$	$\delta^{13}C_{PDB}$ organic	$\delta^{34}S_{CDT}$ pyrite
UA 1	v	26.3	56.1	-13.32	-32.5	-2.56
2	iv	85.7	1.95	-14.17	-33.9	-10.06
3	iii	85.9	1.02	-14.39	-33.2	-20.39
4	ii	87.6	0.90	-14.30	-32.8	-24.28
5	i	87.5	0.79	-13.77	-33.5	-24.01
6	ii	87.1	0.81	-13.73	-33.5	-16.84
7	iii	86.5	0.90	-13.90	-33.4	-17.88
8	iv	86.5	1.53	-14.15	-32.3	-11.27
9	v	25.6	57.6	-12.90	-32.1	-3.04
Weighted average composition		73.0	13.4	-14.06	-	-3.63
UA Host Sediment (average of 3)		5.77	7.16	-6.80	-33.2	-25.76
UB 1	vi	53.6	27.1	-13.68	-35.6	-4.99
2	v	74.1	6.47	-14.99	-32.6	-7.12
3	iv	87.4	2.34	-15.05	-29.9	-13.42
4	iii	84.7	1.95	-15.22	-30.9	-13.32
5	ii	81.4	2.00	-15.26	-30.0	-13.32
6	i	84.2	3.70	-15.27	-29.3	-8.05
7	ii	85.4	2.06	-15.19	-28.7	-11.25
8	iii	85.0	2.13	-15.44	-29.4	-13.05
9	iv	84.7	2.38	-15.29	-26.1	-12.20
10	v	81.2	5.41	-15.26	-29.9	-8.93
11	vi	53.5	23.8	-13.6	-37.0	-5.5
Weighted average composition		77.4	7.50	-15.02	-	-7.28
UB Host Sediment (average of 3)		20.6	7.96	-7.00	-30.4	-24.14

3. *Spatial mineral zonation.*—Calcite occurs within a predominantly pyrite shell.

4. *Textures.*—Calcite occurs as a microsparite cement within the concretions. Pyrite occurs as three different forms: as framboids (throughout the sediment and overgrown and inherited by the concretion), as euhedral crystals (progressively more abundant toward, and heavily concentrated in, the concretion margin), as hopper crystals (in the margins of some concretions and in the host sediments).

5. *Isotopic composition.*—Concretionary calcite has $\delta^{13}C$ −13 to −16 permil, concretionary pyrite ranges from $\delta^{34}S \approx -24$ to −25 permil

(central framboidal phase) but becomes progressively isotopically heavier toward the margin as euhedral pyrite predominates (up to −2 permil).

6. *Host sediment composition.*—Host sediment pyrite is mainly framboidal and is isotopically light (−24 to −25 permil). The parameter DOP

$$\text{DOP} = \text{pyrite Fe}/(\text{HCl-soluble Fe} + \text{pyrite Fe})$$

has an average value of 0.84 in the concretionary horizons. (Raiswell, 1982; Raiswell and others, 1988)

7. *Source of concretionary carbonate.*—The $\delta^{13}C$ of carbonate implies a minimum contribution of half organic-matter carbon ($\delta^{13}C \approx -25$ ‰; for example, Sackett and Thompson, 1963; Schwarcz 1969) mixed with a relatively ^{13}C enriched carbonate, for example seawater derived carbonate ($\delta^{13}C \approx -0$ ‰) to give the resultant $\delta^{13}C \approx -13$ permil.

8. *Ratio of carbonate to pyrite.*—Bulk compositions of the concretions (Raiswell, 1976) show carbonate/sulfide molar ratios for the two concretions are 6.5 and 12.3, respectively. Even if half the carbonate is assumed to be derived from organic matter, the ratios do not accord with the stoichiometry thought to be likely for microbial sulfate reduction (see equations below).

Choice of a Genetic Model

There are several possible models that could be used to explain these observations. In the first instance these differ in the factors that control the siting of concretionary growth. Raiswell (1976) pointed out that siting could be controlled by the existence of suitable nucleation sites in a porewater environment uniformly oversaturated with respect to carbonates. Alternatively, siting might be controlled by the development of regions of locally enhanced supersaturation. These alternatives lead to the following models.

1. *The dynamic model.*—Radial mineralogical zonations here result from spatial variations in porewater chemistry, which are established, because sulfate reduction occurs sufficiently rapidly to produce a microenvironment with locally enhanced concentrations of dissolved sulfide (despite opposing diffusive losses). Once sufficient supersaturation occurred, calcite and pyrite precipitated, and gradients would be established between the microenvironment and surrounding porewaters for all the species involved in reduction of sulfate and precipitation of pyrite. The relative positions of the zones of calcite and pyrite supersaturations are then determined by the relative rates of sulfate reduction, the rates of diffusive additions and losses between the microenvironment and surrounding porewaters, and the rates of calcite and pyrite precipitation. These kinetic controls need not produce coincident zones of calcite and pyrite precipitation.

2. *The equilibrium model.*—Porewaters are uniformly oversaturated with respect to carbonates, and precipitation occurs wherever suitable nuclei are available. Radial mineralogical zonations are then commonly

interpreted as reflecting temporal variations in porewater chemistry during concretionary growth (Raiswell, 1971; Curtis, Coleman, and Love, 1972; Hudson, 1978; Gautier, 1982). On this basis Raiswell (1976) has argued that during growth of the Jet Rock concretions, the porewaters had compositions that initially allowed the precipitation of calcite (accompanied by only small amounts of pyrite) and subsequently allowed the precipitation of pyrite (accompanied by only small amounts of calcite). The precipitation of pyrite at the margin could arise passively or might involve the dissolution of concretionary carbonate (which would locally raise pH and favor pyrite precipitation).

Both models share a common feature, to the extent that carbonate precipitation must be localized and must be separated from pyrite precipitation in either time or space. However both models appear to require that diagenesis in the Jet Rock proceeded in unusual fashion as explained below.

Porewater studies of modern organic carbon-rich sediments almost invariably show high degrees of supersaturation with respect to carbonates (Berner, Scott, and Thomlinson, 1970; Sholkovitz, 1973; Berner and others, 1978). Precipitation however seems to be extremely rare, possibly due to inhibition by adsorbed organic matter and/or phosphate on possible nucleation sites. In the absence of any unequivocal examples of $CaCO_3$ precipitation from modern porewaters, the equilibrium model is viable only if higher supersaturations would ultimately cause slow carbonate precipitation (Canfield and Raiswell, 1991b). There is also a further difficulty in that supersaturation needs to remain poised at a level that allows the use of only a relatively few nuclei in the sediment (in order to produce discrete rather than continuous cementation). The nature of these nuclei and reasons for their selection are entirely conjectural. Certainly the concretions preserve no evidence of any distinct nuclei, apart from skeletal carbonate debris which are readily available throughout the sediment.

It was this difficulty that led Raiswell (1976) to argue that carbonate supersaturation was locally elevated at the concretionary site, to the point where precipitation occurred. The mass balance and stoichometric requirements of this dynamic model have not been explored in detail, although it too may require that diagenetic processes proceed in ways that are unusual compared to modern sediments. It is important therefore to emphasize that, despite the abundance of modern sediment studies, there have been no discoveries of carbonate concretions similar to those found in the geological record. Thus their existence compels us to explore unusual diagnetic mechanisms. In this paper we will evaluate the dynamic model, using the coupled diffusion and precipitation approach of Raiswell and others (1993) to describe the spatial variations in porewater chemistry needed to produce the observed mineral zonations. A subsequent contribution will describe the alternative equilibrium model and evaluate its advantages and disadvantages. Here, however, we begin

evaluation of the dynamic model by examining the stochiometric links between the processes of sulfate reduction and pyrite formation and their influences on carbonate saturation state.

STOICHIOMETRY OF REACTIONS

The following are not typical equations that represent reaction mechanism but net mass balances that summarize the effects of chemical reactions and hence deduce which components produce carbonate supersaturations. We discuss below a wide range of reactions, each of which has the potential to modify the carbonate saturation state. These reactions can be written either in terms of OH^- or H^+. For this paper the convention of using H^+ only has been adopted, but both forms of the first equation are shown below to demonstrate the principle.

Sulfate Reduction (SR)

Microbial sulfate reduction can occur using sedimentary organic matter (or methane) as a substrate,

$$2CH_2O + SO_4^{2-} \rightarrow 2HCO_3^- + HS^- + H^+ \qquad \text{SR------(1 - } H^+ \text{ form)}$$

$$2CH_2O + SO_4^{2-} + OH^- \rightarrow 2HCO_3^- + HS^- + H_2O \qquad \text{SR-----(1 - } OH^- \text{ form)}$$

Where a large proportion of the H_2S is undissociated, the more usual form of the equation is

$$2CH_2O + SO_4^{2-} \rightarrow 2HCO_3^- + H_2S \qquad \text{SR-----(1)}$$

Laboratory and field studies (Aller and Yingst, 1980; Westrich, 1983) have validated the above reaction stoichiometry. Methane may be used as a substrate in a minor, contributory process, Anaerobic Methane Oxidation (AMO).

$$CH_4 + SO_4^{2-} \rightarrow HCO_3^- + H_2S + OH^- \qquad \text{AMO-----(2)}$$

There are no known organisms capable of using methane as a sole carbon source, but there is good evidence for the occurrence of methane oxidation using sulfate as an oxidizing agent either directly or indirectly via reactions coupled to other substrates (Devol and Ahmed, 1983; Reeburgh, 1983). Thus the overall stoichiometry of AMO may not be as simple as that given above.

Iron Reduction (FeR)

Coleman (1985) has shown that SR could either increase or decrease pH, depending on the availability of iron. Ferric-iron-bearing phases can be microbially reduced (Curtis, 1977; Lovley, Chapelle, and Phillips, 1990), and the process involves considerable consumption of H^+, which

may assist the precipitation of carbonates

$$4FeOOH + CH_2O + 7H^+ \rightarrow 4Fe^{2+} + HCO_3^- + 6H_2O \quad FeR\text{-----}(3)$$

Iron Sulfide Precipitation

The following equations are all constructed to examine the effects of different mechanisms of iron sulfide precipitation on the carbonate system. Each mechanism has been modelled using Solmineq (Kharaka and others, 1988). However, model predictions of carbonate saturation states are only approximate, for a variety of reasons. Firstly, organic matter is expressed as CH_2O rather than as the Redfield stoichiometry $(CH_2O)_{106}(NH_3)_{16}(H_3PO_4)$, although degradation of the latter clearly produces protolytic species that will influence carbonate equilibria. Secondly, a closed system is assumed, whereas natural pore systems are open to diffusive exchange with overlying seawater to an extent that varies between different chemical species, depending on their concentration gradients and diffusion coefficients. Thirdly, marine pore waters contain other protolytic species apart from those considered here (for example, borate) which will also influence the carbonate system. Despite these simplifications, the models are adequate enough to demonstrate gross variations in carbonate saturation states that arise through different mechanisms of iron sulfide precipitation (fig. 1). In several cases the simple models used here have been cross-checked against the more refined models used by Canfield and Raiswell (1991b), and comparable results were obtained. The closed system models used here are also consistent with the open system models of Boudreau and Canfield (1993), except as noted above.

Different equations can be written for the formation of FeS (which is taken to represent a pyrite precursor) depending on whether FeR and SR occur together at the same site or whether the product of one reaction (Fe_{2+} or dissolved sulfide) migrates to the site of the other. Iron sulfide precipitation can be represented as

$$Fe^{2+} + H_2S \rightarrow FeS + 2H^+ \quad (4)$$

where Fe^{2+} reacts with H_2S, both in solution.

Hence, where FeR and SR occur together, we can combine (1), (3), and (4) to determine the overall effect.

$$9CH_2O + 4SO_4^{2-} + 4FeOOH \rightarrow 9HCO_3^- + 4FeS + 6H_2O + H^+ \quad (5)$$

Conversely, where FeR and SR are separated, precipitation of FeS has an overall effect given by (1) and (4).

$$2CH_2O + SO_4^{2-} + Fe^{2+} \rightarrow FeS + 2HCO_3^- + 2H^+ \quad (6)$$

The equations above refer to formation of FeS which is the product observed to be forming in Recent anoxic muds (Berner, 1970; Goldhaber

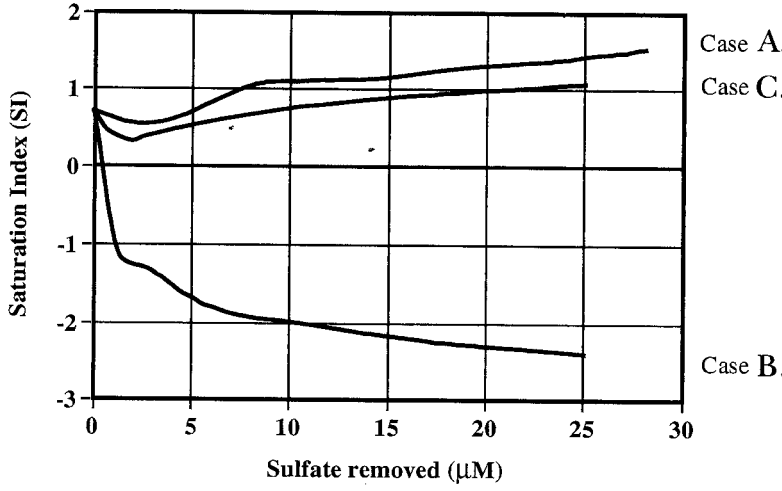

Fig. 1. Carbonate saturation in the sediment, modelled to show the effects of different modes of sulfate reduction and iron sulfide precipitation.

Case (A) represents HCO_3^-/H^+ in the ratio 9:1, simultaneous FeR and SR to precipitate FeS (eq 5)

Case (B) represents HCO_3^-/H^+ in the ratio 1:1, SR with remotely reduced iron to precipitate FeS (eq 6)

Case (C) represents addition of $6HCO_3^-$, SR with remotely reduced iron to precipitate FeS_2 (eq 12). Half the S^o is supplied in situ from iron oxides.

and Kaplan, 1974), although pyrite is the diagenetic end-product. This transformation involves an increase in oxidation state of sulfur from FeS to FeS_2 and may actually involve incorporation of partially oxidized sulfur species. Regardless of the precise reaction pathway, the net effect can be represented *for mass balance* by the following equation.

$$FeS + S^o \rightarrow FeS_2 \qquad (7)$$

The precise mechanism by which most S^o (or other partially oxidized sulfur species) forms is unknown, although the oxidation of H_2S by iron oxides (Pyzik and Somner 1981; Canfield, 1989) is often very important during shallow burial.

$$H_2S + 2FeOOH + 4H^+ \rightarrow S^o + 2Fe^{2+} + 4H_2O \qquad (8)$$

or

$$2CH_2O + 2FeOOH + 4H^+ + SO_4^{2-} \rightarrow S^o + 2Fe^{2+} + 2HCO_3^- + 4H_2 \qquad (9)$$

Oxygen is an unlikely electron acceptor in non-bioturbated sediments like the Jet Rock. The net reactions represented by eqs (8) and (9) are large alkalinity producers by consumption of H^+ and, in the case of (9), by production of HCO_3^-.

An alternative recently documented transformation process (Drobner and others, 1990) uses the oxidation of H_2S to form H_2

$$FeS + H_2S \rightarrow FeS_2 + H_2 \quad (10)$$

Molecular hydrogen is a preferred electron donor for many anaerobic microbes which would use it to reduce a variety of oxidized species in the sediment (including CO_2, FeOOH, SO_4^{2-}). Some of these reactions might also generate alkalinity.

Eqs (5) and (6) can be modelled as a closed system using SOLMINEQ (Kharaka and others, 1988) simply by adding/removing dissolved products in the correct stochiometric proportions relative to sulfate (but without precipitating carbonate). As would be expected, eq (5) produces carbonate supersaturation, and eq (6) quickly establish a high degree of undersaturation.

Pyrite however should be the end-product of FeR plus SR in eq (5), and thus, effectively 4 moles of S^o need to be generated from eq (9) to permit the transformation of FeS to FeS_2. Formation of each mole of S^o consumes $4H^+$ (eq 8) and also generates alkalinity, and thus the effects of adding eqs (5) and (9) will be to cause additional carbonate oversaturation, over and above that already modelled in figure 1, case (A). The overall process rapidly consumes iron oxides and occurs in iron-rich porewaters (see eq 13, below). Clearly it can occur only as long as iron oxides are available, and it would correspond mainly to the formation of the pre-concretionary framboidal pyrite.

Concretionary growth, once initiated, was accompanied by small concentrations of euhedral pyrite which occur in the core of the concretion. It is reasonable to expect that small concentrations of iron could continue to be sourced from in situ oxides to precipitate pyrite directly

$$3H_2S + 2FeOOH \rightarrow FeS + FeS_2 + H_2O \quad (11)$$

However iron sources would have become limited and it seems unlikely that enough iron would have been available to generate the necessary S^o from the process described by eq (9) to complete pyrite formation. An external source of S^o may have been required for 50 percent of the pyrite formation. Note that SR would have been needed to form the H_2S in eq (10), and the overall result was therefore

$$6CH_2O + 3SO_4^{2-} + S^o + 2FeOOH \rightarrow 6HCO_3^- + 2FeS_2 + 4H_2O \quad (12)$$

The effect on the carbonate equilibria was to produce a substantial degree of oversaturation (fig. 1, case C). Still higher supersaturations than this would have resulted if more than 0.5 S^o was formed from iron oxides.

These results demonstrate that, provided iron oxides were available to form partially oxidized sulfur species, the direct precipitation of pyrite generated extensive carbonate supersaturation. However this situation could not have been maintained indefinitely, and the large masses of

pyrite in the concretion margins necessitated an external source of iron (eq 6).

Most Significant Effects on the Carbonate Buffer

It is apparent from the mass balances described by the equations above that some reactions consume H^+ while others generate it. Obviously, generation of H^+ will dissolve carbonate or at least lower carbonate supersaturation. However, although sulfate reduction may occur, precipitation of carbonate associated with the process will be controlled by:

1. Whether FeR and SR are coincident in both space and time.
2. The rate of FeR relative to SR.
3. Whether pyrite forms directly or via FeS

The following section will identify the most probable combinations of these alternatives in the Jet Rock and their implications as to the equilibrium or dynamic models.

MECHANISMS OF CONCRETIONARY PYRITE AND CALCITE FORMATION: IMPLICATIONS FOR THE GROWTH MODEL

Pyrite

The concretioins contain the following phases of diagenetic pyrite: first a framboidal phase (equally abundant in the host sediments and concretions, after the latter are corrected for the dilution effect of the carbonate cement). Second, there is euhedral pyrite, which first nucleates on, and then progressively envelopes, the framboidal pyrite. This euhedral pyrite becomes more abundant toward the concretion margin and is characteristically associated with concretionary growth (Coleman and Raiswell, 1981; Raiswell, 1982). Third, some concretions have hopper pyrite crystals embedded in their pyritiferous margins (Carstens, 1985). These are clearly the last phase of pyrite to form at the concretion site, and their absence from many concretions indicates that they are not necessarily associated with the growth process.

The formation of a framboidal phase is usually taken to indicate the necessary involvement of an FeS intermediate (Sweeney and Kaplan, 1973). Its growth rapidly and early in the diagenetic burial sequence implies precipitation from pore fluids with a high degree of supersaturation. This fact, together with the pyrite texture, suggests it to be the result of active SR associated with rapid FeR.

However the euhedral phase of pyrite, which forms later than the framboidal phase (both textural and isotopic evidence), is believed to have precipitated directly (Raiswell, 1982), under conditions where limitations on the iron supply allowed supersaturation with respect to pyrite but under-saturation with respect to FeS (Goldhaber and Kaplan, 1974). Direct precipitation is believed to be possible provided pyrite nuclei are available (Schoonen and Barnes 1991). There is clear evidence within the concretion of euhedral pyrite nucleating around framboidal pyrite (Raiswell, 1982). Furthermore the bulk molar ratios of calcite to pyrite in

the two concretions are 6.5 and 12.3. This represents an excess of carbonate over sulfide compared to the stoichiometric value of 2 (in eq 1). This may represent addition of HCO_3^-, however if it indicates loss of H_2S, this would show that growth of pyrite was limited by supply of Fe from an external source. In addition, Carstens (1985) has concluded that the hopper morphology also arises from diffusion-controlled growth, due to limitations on Fe supply. These arguments suggest that the overall reaction at the concretion site is given by a combination of a high rate of SR (and/or AMO) which generated sulfide more rapidly than iron could be supplied from external sources for the direct precipitation of pyrite.

Calcite

As detailed in the *Sample Description* section above, diagenetic calcite is present as a single microsparite phase, the precipitation of which can be very precisely timed relative to the different phases of pyrite formation. Precipitation of the concretionary carbonate must have post-dated the growth of framboidal pyrite (which is found inside all the concretions); however the radially increasing concentrations of euhedral pyrite strongly suggest that formation of the concretionary carbonate accompanied that of the euhedral pyrite (Coleman and Raiswell, 1981). It is difficult to envisage the alternative: that euhedral pyrite was added later (to a pre-existing carbonate concretion) by fluids that penetrated to the center of the concretion and precipitated pyrite *without leaving any textural evidence for carbonate dissolution or replacement.* Clearly however, assuming replacement did not occur, it is necessary to explain why carbonate precipitation was only associated with euhedral pyrite and why euhedral pyrite is localized as a shell around the concretionary carbonate and not distributed uniformly through it.

In a spatial model the precipitation of carbonate is governed both by saturation state of dissolved carbonate and kinetic factors. Each of the steps associated with the precipitation of precursor FeS (eq 5) and its transformation to framboidal pyrite (via S^o, eq 8) produces alkalinity, so that there will be a substantial increase in carbonate supersaturation. However, framboidal pyrite precipitated under open system conditions (see later, also Coleman and Raiswell, 1981) which facilitated loss of alkalinity. This effect was clearly sufficient to prevent the precipitation of pre-concretionary carbonate, although the precise carbonate saturation state cannot be determined.

Subsequently, carbonate supersaturation must have occurred at the concretion site, although the extent of this would depend on how partially oxidized sulfur species were generated. We have also argued that the rate of sulfate reduction exceeded the diffusive supply of iron to the concretion site, thus the state of saturation depended on the superimposed effects of the rate of sulfate reduction (eq 1) and the rate and mechanism of pyrite precipitation.

Summary of Key Reactions

The appropriate equations are combined here to explain the key observed features of pyrite precipitation and show their net effect on the sulfide and carbonate systems. Although they show the dominant process for each major stage, the actual pore-water compositions would have been modified by the surviving products from all previous reactions.

1. *Pre-concretionary state (framboidal pyrite).*—

$$17CH_2O + 8SO_4^{2-} + 12FeOOH + 15H^+ \rightarrow$$
$$17HCO_3^- + 4FeS_2 + 8Fe^{2+} + 22H_2O \quad (13)$$

Addition of eqs (5) and (9) shows the effects of an initial phase of uniform SR and associated FeR (using in situ sources of iron to form S^o, which is used to transform FeS to FeS_2). Alkalinity was generated, but pore waters were open to the overlaying seawater (see later) and did not become sufficiently supersaturated for carbonate precipitation to occur. Iron-rich porewaters occurred during this phase of diagenesis (Canfield and Raiswell, 1991a).

Rates of sulfate reduction were not homogeneous, and sites where rates were higher than in the surroundings become the incipient concretions.

2. *Concretionary growth site (euhedral pyrite in concretion core).*—At this stage rates of H_2S production exceeded rates at which iron could be supplied in situ, from the remaining clastic phases. Euhedral pyrite was directly precipitated using in situ sources of iron to form some S^o (via eq 8) which was precipitated directly as pyrite. An additional external S^o source was required in eq (13) as in situ sources were limited, The deficiency of iron also allowed surplus H_2S to diffuse outward.

$$6CH_2O + 3SO_4^{2-} \rightarrow 6HCO_3^- + 3H_2S \quad (14)$$

$$3H_2S + 2FeOOH + S^o \rightarrow 2FeS_2 + 4H_2O \quad (15)$$

A further unknown source of S^o was required to directly precipitate at least 50 percent of the pyrite, and the origin of this remains speculative (see earlier). This process need not have generated alkalinity and may have been broadly neutral in its effect on the carbonate equilibria. As long as at least 50 percent of the pyrite utilized S^o derived via local reduction of iron oxides, then the alkalinity generated would produce carbonate supersaturation and precipitation. Nevertheless, rates of precipitation were not so fast as to produce a local depletion of carbonate at the concretion site compared to its surroundings.

3. *Concretionary growth site (euhedral margin).*—The above growth phase continued until the outward diffusion of H_2S was diminished enough to match the inward diffusion of iron from the surrounding porewaters. In situ sources of iron had been exhausted, but precipitation of euhedral pyrite occurred using the outward diffusing H_2S and the

inward diffusing Fe^{2+}.

$$Fe^{2+} + S^{o} + H_2S \rightarrow FeS_2 + 2H^{+} \quad (16)$$

The surrounding porewaters were required to supply a dissolved partially oxidized sulfur species (represented as S^{o}). The processes generating Fe^{2+} (and S^{o}) in the surrounding sediments also generate alkalinity (eqs 3 and 8) which buffered the H^{+} generated above and allowed carbonate precipitation to continue inside the euhedral pyrite rim. The removal of alkalinity at the concretion site diminished supersaturation in the surrounding porewaters, making precipitation less likely and thereby amplifying self-organization.

An alternative, but highly speculative, mechanism, which would not require supply of S^{o} from the host sediment, is direct precipitation of pyrite using a combination of the mechanisms given in eqs (4) and (10).

$$Fe^{2+} + 2H_2S \rightarrow FeS_2 + H_2 + 2H^{+} \quad (17)$$

This too would amplify self-organization in the same way as mentioned above. All the stages represented are summarized in figure 2.

THE DYNAMIC MODEL FOR CONCRETIONARY GROWTH

Host Sediment prior to and during Concretionary Growth

The inferences drawn in the previous sections can be integrated into a model for conretionary initiation and development consistent with observations of the chemical variations in modern anoxic sediments and their pore waters. A recent review of the sedimentary geochemistry of Long Island Sound, Mississippi Delta, and the Santa Barbara Basin shows common features of pore water and solid phase chemistry (Canfield and Raiswell, 1991a). A near surface zone where pore water concentrations of iron are high and total dissolved sulfide is low overlies a sulfide-rich/iron-poor zone. In the upper zone the relatively rapid rate of reduction of reactive iron oxides exceeds the rate of SR, hence dissolved sulfide is reacted from solution forming iron sulfides. However, as iron oxides are consumed, sulfide levels rise, and the concentrations of dissolved iron fall in response, creating the lower, sulfide-rich zone.

Observations of the concretions can be related to a similar paleo–porewater system, and their formation is most readily attributed to the region near the boundary between the two zones. Thus, the characteristic feature of concretionary growth is the precipitation of euhedral pyrite, whose presence implies direct precipitation (Raiswell, 1982). This requires that pore waters at the concretion site were poised such that the sulfide saturation state exceeded that of pyrite (approx 2.4×10^{-28}, moles^2 liters^{-2}; Goldhaber and Kaplan, 1974) but not that of any FeS phases (approx 10^{-18} moles^2 liters^{-2}; Berner, 1967). The saturation states

for pyrite and FeS are defined by the reactions as given in eqs (18) and (19).

$$Fe^{2+} + S^{o} + S^{2-} \rightarrow FeS_2 \quad (18)$$

$$Fe^{2+} + S^{2-} \rightarrow FeS \quad (19)$$

However the pore waters must also have been capable of supplying substantial amounts of dissolved iron to form the concretionary pyrite, even though the earlier formation of framboidal pyrite had considerably depleted reactive iron from nearby sediments. These arguments indicate that the pore waters probably had a low but significant activity of dissolved iron, but a still lower activity for the sulfide ion. These conditions would only have occurred at the base of the iron-rich zone or the top of the sulfide-rich zone (provided low pH values limited sulfide ion activity). Canfield and Raiswell (1991a) find this transition zone to be no more than about 10 cm thick (compared to a typical concretion thickness of 20 cm), but it is very difficult to know whether these steady state porewater systems fairly represent the non-steady-state conditions under which concretionary growth might have occurred (Raiswell, 1978). Estimated growth rates (Coleman and Raiswell, 1993) imply a pause in sediment deposition was necessary for growth to have occurred.

DEVELOPMENT OF THE SPATIAL ZONATION MODEL

The position where precipitation of pyrite occurs will depend on the relative sizes of the dissolved iron and dissolved sulfide ion activities. Supersaturation will occur over that radial distance where the concentrations of the inward-diffusing dissolved iron and the outward-diffusing sulfide ion (whose activity is controlled by the equilibria between HCO_3^-, H^+, and HS^-) give an ion activity product that exceeds the solubility product of pyrite. The results of diffusion and reaction may produce a spatial distribution of products characteristic of the sytem. The model of Raiswell and others (1993) describes the spatial distribution of a precipitate produced from reaction of two solutes. In the model, one solute diffuses out from a small, spherical reservoir volume into a surrounding infinite reservoir of the other solute. The model is not a perfect analogue of the sedimentary system, since it assumes both reservoirs are infinite. Despite the minor shortcomings of the model it illustrates the effects of a reaction-driven diffusion system and can explain the observed features of the concretionary system. This is probably the best that can be done in modelling a diagenetic rock system as opposed to a modern sediment, where transient phases and pore water parameters can be measured directly. More details are given in app. 1, but the model can be used to show how the size, shape, and position of the steady state, diffusion-controlled, rate of precipitation of pyrite varies in the space between the two reservoirs, containing different concentrations of dissolved sulfide (at the concretionary site) and dissolved iron (in the surrounding porewaters).

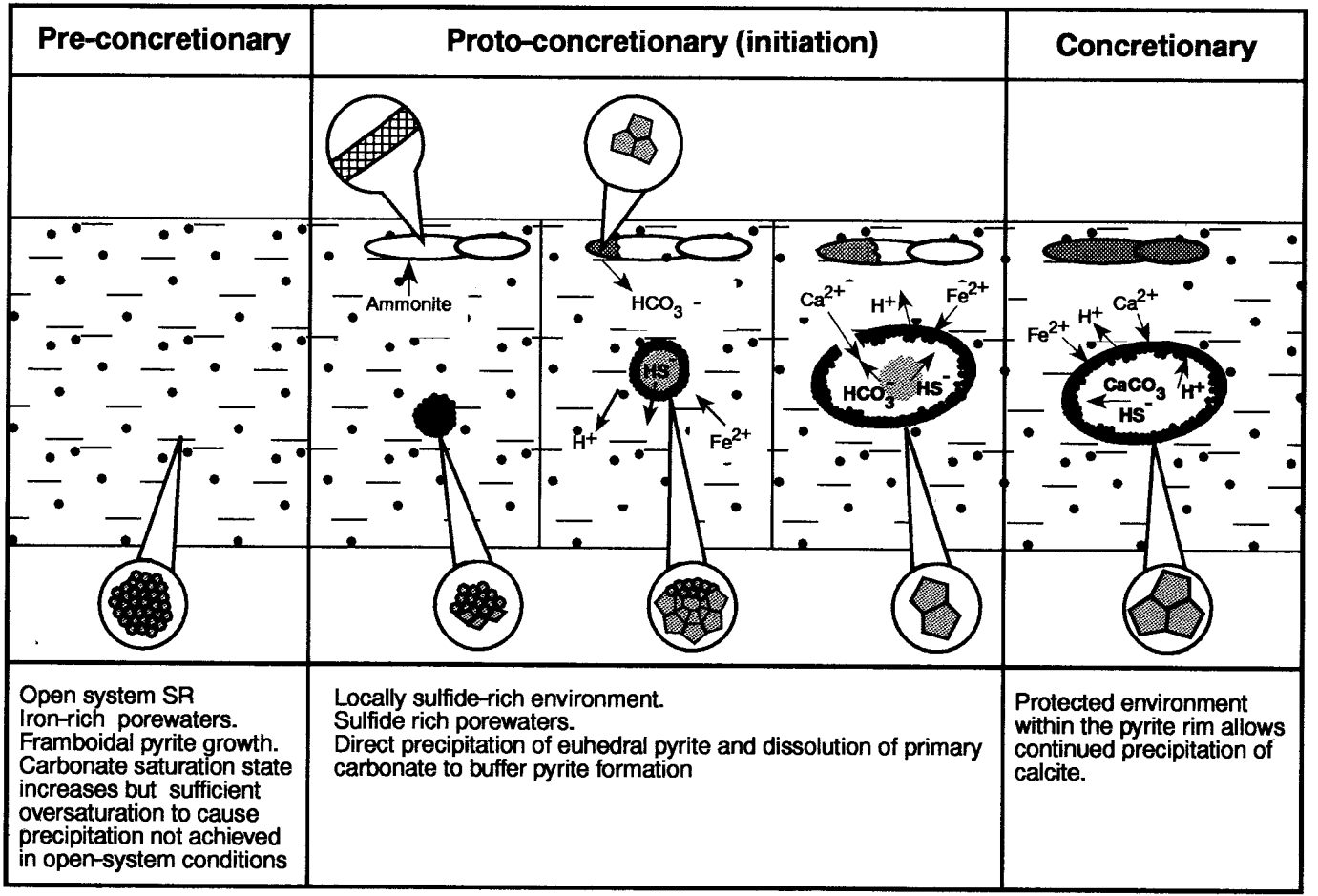

Fig. 2. The division of the environment into two zones at the time of initiation of concretionary growth allows eventual precipitation of carbonate within the concretionary volume.

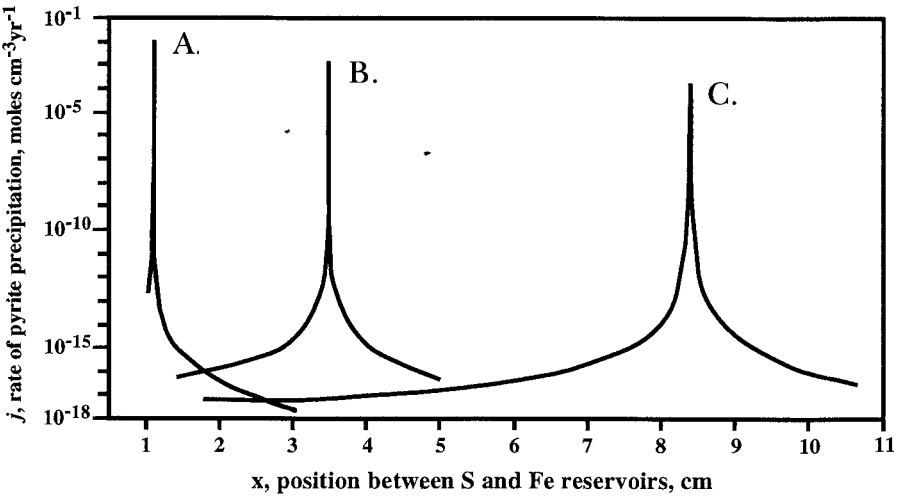

Fig. 3. Diffusion with precipitation models. Based on the model of Raiswell and others (1993), the rate of pyrite precipitation (j) is shown relative to its position (x) between the sulfide and ferrous iron reservoirs separated by a distance (d). In each of four cases j is plotted only where the condition for precipitation is met; $C_S \times C_F > 2K$.

Case (A) $C_S = 1 \times 10^{-10}$, $C_F = 2.5 \times 10^{-9}$ mol cm^{-3}; $C_S C_F = 2.5 \times 10^{-19}$.

Case (B) $C_S = C_F = 2.5 \times 10^{-9}$ mol cm^{-3}; $C_S C_F = 6.3 \times 10^{-18}$.

Case (C) $C_S = 7.3 \times 10^{-9}$, $C_F = 2.5 \times 10^{-9}$ mol cm^{-3}; $C_S C_F = 1.8 \times 10^{-17}$. With equal concentrations of sulfide and iron the precipitation maximum is offset toward the iron reservoir (compare cases A and B). Where there are different sulfide and iron concentrations, the zone of precipitation moves toward the reservoir of lower concentration (compare cases A and C).

Three separate scenarios have been modelled to demonstrate how the magnitude, position, and intensity of precipition vary. The results are shown in figure 3. Following the argument of Helfferich and Katchalsky (1970), the work of Raiswell and others (1993) and Coleman and Raiswell (1993) show that precipitation *only* occurs between the two reservoirs when

$$C_S^o \times C_F^o > 2K,$$

where C_S^o and C_F^o are initial reservoir concentrations of dissolved sulfide and iron respectively (moles cm^{-3}), and K is the solubility product of the pertinent reagent species. Coleman and Raiswell (1993) showed how variations in the ratio of C_S^0/C_F^o and the product $C_S^o \times C_F^o$ control the position and thickness of the zone of pyrite formation. The examples shown in figure 3 are for the precipitation of pyrite at pH 7.5 and have the product $C_S^o \times C_F^o$ in the range 10^{-17} to 10^{-19} (in excess of the saturation level for pyrite but below that for FeS; see Raiswell and others, 1993). The saturation values are defined with respect to HS^- and should not be confused with those defined for S^{2-} (eqs 18 and 19). The most

important feature of figure 3 is that the zone of pyrite formation moves outward from the center of the sulfide reservoir as the ratio C_S^o/C_F^o increases, Where the reservoir concentrations are equal the precipitation maximum is offset toward the iron reservoir, because the diffusion coefficient for iron is less than that for sulfide (compare curves A, B, and C). The precipitation zone also tends to become thicker for larger values of the product $C_S^o \times C_F^o$, but model derived zone thicknesses of the size actually observed in the Jet Rock concretions require the existence of some oversaturation in the precipitation zone (Coleman and Raiswell, 1993).

Clearly the position and thickness of the zone of pyrite precipitation will depend on the concentrations of dissolved sulfide (and thus the rate of sulfate reduction) at the concretionary site and the concentrations of dissolved iron in the porewaters. These variables cannot be quantified, but there is good evidence to suggest that $C_S^o > C_F^o$. Thus, as argued previously, the formation of framboidal pyrite in these sediments consumed the most reactive iron phases, and hence the formation of the margin of euhedral pyrite drew upon residual sources of iron transported from adjacent sediments. It also has been argued (see earlier) that concentrations of dissolved iron in porewater were low. Additionally, SR at the concretionary site clearly proceeded fast enough to establish local carbonate supersaturation. Hence, rates of sulfide production must have exceeded rates of diffusion initially, with the consequence that high concentrations of dissolved sulfide must have occurred at the concretionary site. In this respect case (C) is most likely to describe the position and shape of the zone in which pyrite precipitated (but see Coleman and Raiswell, 1993). This curve shows that pyrite precipitation does *not* occur uniformly between the two reservoirs but is heavily concentrated immediately adjacent to the reservoir of dissolved iron at the outer margin of the concretion (note the logarithmic scale in fig. 3). Clearly the precipitation of carbonate must have occurred contemporaneously, inside the growing pyrite shell, due to the alkalinity generated there by sulfate reduction. The progressive radial variations in the calcite/pyrite ratio do not therefore record *temporal* changes in porewater chemistry during concretionary growth. Instead they define *spatial* variations in the mineral saturation states arising from the interaction between the concretion microenvironment and its surroundings.

EVALUATION OF THE MODEL: (1) OBSERVATIONS THAT SUPPORT THE MODEL

A number of other observations support and constrain this hypothesis to varying degrees. Rate of burial has been postulated to be a major control on which specific process dominates in any particular bed (Coleman, Curtis, and Irwin, 1979; Pisciotto and Mahoney, 1983). An increase in burial rate would diminish replenishment of sulfate from overlying seawater and decrease sulfide production rate. Carstens (1985) has concluded that the hopper morphology seen in the euhedral pyrite arises from diffusion-controlled growth, due to limitations on Fe supply, but

equally it could be caused by restriction of sulfide. However, occurrence of concretions only in a limited number of stratigraphic horizons also implies that sediment accumulation rate is not the only control and that perhaps sediment type might be an important control too. These possibilities are evaluated critically below.

Vertical Distribution of Concretions in the Section

The details of SR process given by pyrite texture and sulfur isotopic composition require a very specific burial scenario. A period of open system SR to produce framboidal pyrite (from iron monosulfide) with constant isotopic composition suggests a relative pause in burial with the relevant bed held in diffusive contact with overlying seawater. The change to direct precipitation of pyrite (with less negative sulfur isotope composition) required that sulfate replenishment be limited.

Although a pause in sediment deposition is necessary for the model, there is no definitive evidence that it occurred. However, sediment lamination texture (O'Brien, 1990) suggests that this possibly might have occurred. Beds 33 and 37, the concretionary horizons, have thick lamination and represent nearer-shore environments with relatively-rapid sediment accumulation. In both cases the beds above them (35 and 39, respectively) have wavy lamination and indicate a change to deeper water conditions with growth of bacterial mats at the sediment water interface. Deeper water implies a reduction in sediment accumulation rate as does the prominence of bacterial mats. The reduction in sediment-accumulation rate would hold the concretionary beds in the SR zone (see above and Raiswell, 1987).

The bacterial mats may also have been important in acting as a chemical sink for dissolved sulfur species, due to the intense activity of sulfur-oxidizing bacteria (Jorgensen and Revsbech, 1983) and sulfate reducers (Canfield and Des Marais, 1992), which they may host. Thus, if sufficiently thick, the mats may have encouraged the development of isotopically-heavy sulfide at depth, if their consumption of sulfide accelerated its removal from the concretionary site, or if their consumption of sulfate constrained diffusive supply to the concretionary site.

Pyrite Replacement of Aragonitic Shells

With the exception of the carbonate precipitated diagenetically, forming the concretions, there is very little other carbonate in the sedimentary unit. This is consistent with the generation of H^+ as a result of early diagnetic reactions (for example, eqs 4 and 5). However, it is plausible to postulate that reactions that generate H^+ need its consumption in order to continue. Therefore, after more-available (finer grained) carbonate has been consumed, then those reactions can proceed only in the presence of a buffer to consume H^+. It is possible that precipitation of massive (non-framboidal) pyrite (eq 16) can occur only in the presence of carbonate. The replacement of ammonites by pyrite is consistent with this model of pyrite precipitation and in that case would be an essential

prerequisite for, rather than a chance by-product of, continued sulfate reduction.

Lateral Distribution of Concretions in a Bed

The mechanism proposed for pyrite precipitation at the margin of the concretion also requires diffusion of H^+ away from the site of concretionary growth (see fig. 2). Its presence would inhibit precipitation of carbonate in the immediate vicinity. Support for this effect can be found in the low proportion of coalesced concretions and the nearest-neighbor distances for the two beds (Raiswell and White, 1978) which shows that the concretions are distributed randomly in the bed.

Carbon Isotope Composition of Concretionary Calcite

The two characteristic components that contribute to diagenetic carbonate are organic matter ($\delta^{13}C \approx -25$ permil) and marine carbonate, present as both dissolved bicarbonate and biogenic shell material ($\delta^{13}C \approx 0$ permil). The data in table 1 show that the concretions have values in the range -15.5 to -12.9 permil. These values are typical of carbonate produced by degradation of organic matter (Curtis, 1977; Irwin, Curtis, and Coleman, 1977) but they are more positive than the organic matter that sourced them: $\delta^{13}C \approx -25$ permil (for example, Sackett and Thompson, 1963, Schwarcz, 1969). Although preceding reactions would have contributed bicarbonate both from organic matter and from dissolution of biogenic carbonate, the key reactions are those that occurred during the period of concretionary growth (eqs 14, 15, 16). Because the concretions contain very much more carbonate than could have been sourced within their own volume, the reaction that caused carbonate supersaturation (eq 1) would have precipitated additionally any other bicarbonate present in solution in porewater within the volume of the concretion (predominantly from dissolution of local biogenic calcium carbonate). At the rim of the concretion (eq 16), generation of organically-derived bicarbonate was matched by H^+ production which was buffered by dissolution of marine carbonate. Precipitation of framboidal pyrite in the host sediment would have resulted in a similar net mass balance, also buffered by dissolution of carbonate. These processes would have given dissolved bicarbonate of approx -12.5 permil (equal parts of the two components). However the additional organic component input (eq 1) would allow more negative values. Thus, the data are consistent with the proposed diagenetic reactions and are similar to values measured by Alperin (1988) in modern low Fe, sulfide-rich porewaters.

Sulfur Isotopic Composition of Pyrite

Isotopic composition of pyrite sulfur varies progressively from light values, -24 permil to -25 permil, for framboidal pyrite (concretion center and host sediment) to heavier ones, up to -3 permil, as the proportion of euhedral pyrite increases. This too can be considered as a two component mixture. SR produces sulfide 42 permil more negative

than the original sulfate (Chambers and Trudinger, 1978). Lower Jurassic seawater sulfate had an isotopic composition of about +18 permil which would give sulfide of about −24 permil, the value measured for framboidal pyrite. However, if sulfate supply were restricted, during deeper burial of the sediment, then precipitation of isotopically negative sulfide would have caused concommitant increase in $\delta^{34}S$ of the residual sulfate. In turn, sulfide produced from that sulfate would have been isotopically heavier, as was euhedral pyrite. Thus, sulfur isotope evidence is consistent with a model in which framboidal pyrite was produced early during burial by solutions considerably supersaturated with respect to sulfide, which must have been open to sulfate replenishment, while euhedral pyrite formed at a much lower supersaturation state, as might be expected when depletion of sulfate concentration had occurred.

If a bulk isotopic composition of −4 permil (see table 1) is assumed for the euhedral components of the two concretions, then the approximate extent of sulfate depletion can be calculated. An average euhedral pyrite value of −4 permil implies an average sulfate source 42 permil more positive (Chambers and Trudiner, 1978), +38 permil. Simple Rayleigh fractionation calculations show that Early Jurassic seawater sulfate with $\delta^{34}S$ of +18 permil (Claypool and others, 1981) would have been depleted to about 0.63 of its original concentration (assuming no differential isotopic diffusion; Goldhaber and Kaplan, 1980). This value is similar to the $\delta^{34}S$ value for sulfide measured by Alperin (ms) in sulfide-rich porewaters that could be considered to be the recent equivalents of those that precipitated the sulfide rims of the concretions.

Oblate Shape of Concretions

In the previous sections, accounts have been given as to how concretions might grow in a spheroidal shape. However, although many concretions are spherical, most are oblate spheres, and many display circular symmetry in the horizontal plane but an eliptical, vertical cross section. In all cases the major axis of the vertical section elipse is horizontal, never vertical. This is consistent with a model controlled by radial diffusion of solutes. Burial of mudrocks fairly rapidly results in horizontal orientation of clay minerals (Pettijohn, Potter, and Siever, 1973) which, in turn, gives greater horizontal than vertical permeability (Mast and Potter, 1963). Therefore, centrifugal diffusion of sulfide would cause a slight preferential transport horizontally, giving the observed shape.

Size of Concretions

The main control on the size of a concretion is the ratio of sulfide production rate to availability of Fe^{2+}. A high ratio will imply a greater diffusive distance for dissolved sulfide before saturation with respect to pyrite is exceeded and would give a larger concretion (see fig. 3B and C). A qualitative confirmation of this concept is given by the relative amounts of acid-soluble iron measured in the two concretionary horizons; availability of iron at the time of concretionary growth cannot be related directly

TABLE 2

The relationship of concretion size to availability of iron

Bed no.	Bed name	Max. concretion diameter	Percent Fe_{HCl} Concretion	Percent Fe_{HCl} Host mud
33	Cannonball Doggers	30 cm	0.21	0.70
37	Curling Stones	70 cm	0.12	0.55

to this parameter, but the two should vary sympathetically. The relationships between concretion-size and available iron is shown in table 2.

It can be seen that greater concentration of iron in bed 33 is associated with growth of a smaller concretion, which accords with the model described in the previous section (Quantitative Development of the Model). Taken together, these corollaries of the proposed model form a corpus of supporting evidence but in themselves do not form conclusive proof.

EVALUATION OF THE MODEL: (2) OBSERVATIONS THAT ARE DIFFICULT TO RECONCILE WITH THE MODEL

The model requires:

1. A very specific porewater environment; it is only found over a very limited depth range in modern, organic-rich sediments.
2. A considerable amount of sulfur of intermediate oxidation state (S^o); the precise mechanisms of the relevant supply reactions are obscure.
3. A source of readily metabolisable organic matter to fuel sulfate reduction at the concretionary site; the concretions preserve no evidence of this.
4. A considerable and continuous source of iron; the most reactive iron phases probably would have been utilized before concretionary growth.

CONCLUSIONS

Despite the above difficulties, the dynamic model explains the following features and has application beyond the rocks described here. They are

1. Mineral zonation in these carbonate concretions is spatially and not temporally controlled. The consequence of this is that carbonate concretions formed in this way do not record successive changes in pore-water composition like the sideritic ones reported by Curtis, Coleman, and Love (1986).
2. The sedimentary system initially existed as a heterogeneous mix of oxidized inorganic species and reduced organic ones. Some of its chemical potential was realized by reaction in self-organized domains. One particular adjunct to this was that carbonate was precipitated in extremely confined locations, while carbonate dissolution occurred in other parts.

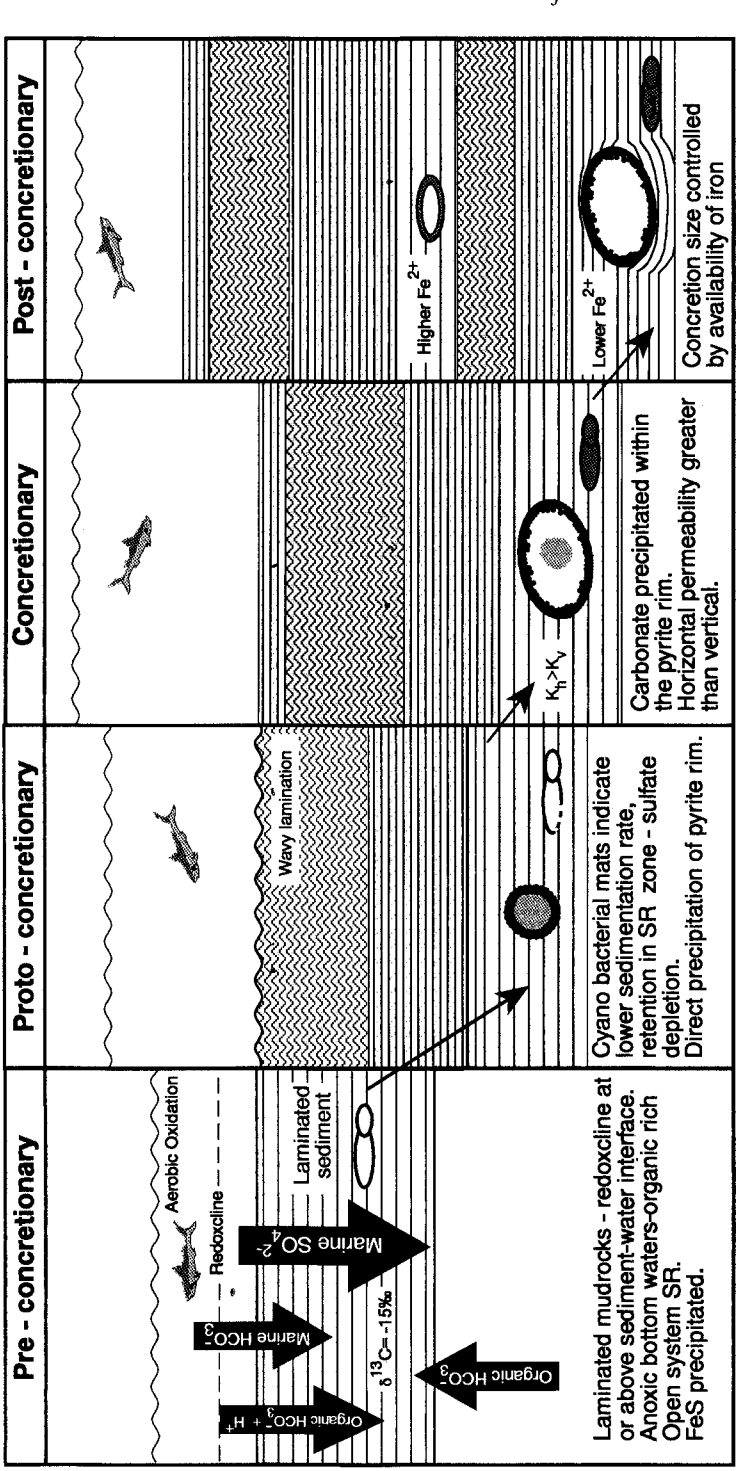

Fig. 4. The chemical environments shown to be necessary for concretionary growth are related to the sedimentological conditions believed to have fostered them.

3. The dynamic model for concretionary growth differs from most descriptions of diagenetic processes, which are formulated as steady state chemical systems. In the diffusive model an initial transient state establishes the bounds of the system, and only subsequently does it rapidly lead to a steady-state system.

4. The model implies a specific sequence of sediment accumulation rates and bottom water environments to allow growth of concretions within the sediment. This may explain why concretions of the type described here have not yet been observed in the process of formation in Recent sediments. The hypothetical association with bacterial mats and a decreased sedimentation rate give a prediction from the model which may be tested in the future.

These features are summarized in figure 4.

ACKNOWLEDGMENTS

We are very grateful to Mandy Muggeridge of BP for turning sketched ideas into drafted figures. We are indebted to Bob Berner, Bernie Boudreau, Don Canfield, Charles Curtis, and Lynn Walter for constructive criticism which has greatly improved the clarity of presentation of our ideas.

APPENDIX I

This model of Raiswell and others (1993) is a modification of the treatment of diffusion plus precipitation by Helfferich and Katchalsky (1970). Although it is not a perfect analogue of the system, it can be used to show how the locus of pyrite formation varies with porewater chemistry and sulfate reduction rate. The model envisages the existence of two infinite reservoirs which predominantly contain dissolved iron (representing the porewater chemistry) and dissolved sulfide (representing the microenvironment where organic matter is degraded by sulfate reduction). It is assumed that;

1. Mass transfer occurs only by diffusion and is unaffected by electrostatic interactions between the ions. This is reasonable where the reacting ions have equal valencies (Helfferich and Katchalsky, 1970).

2. The rate of precipitation is controlled by diffusional supply of the reactants; that is, supersaturation and equilibrium are not instantaneous (see earlier).

3. Precipitation does not impede diffusion. This is probably a safe assumption only for the early stages of precipitation.

4. A single reactant predominates in each reservoir, the compositions of which remain constant. This is a reasonable assumption given the low solubility products for iron sulfides.

The model gives a function for rate of precipitation,

$$j = \frac{2a^2(D_S C_S^o + D_F C_F^o)^2 D_S D_F K}{r^4\{[D_F C_F^o - (a/r)(D_S C_S^o + D_F C_F^o]^2 + 4D_S D_F K\}^{3/2}}$$

where

j = rate of precipitation (moles cm^{-3} yr^{-1}) at r
r = distance from the center of the spherical reservoir (cm)
a = radius of spherical reservoir (cm)
D_S, D_F = diffusion coefficients for dissolved sulfide and dissolved iron, respectively (cm^{-2} yr^{-1})

C_S^o, C_F^o = initial reservoir concentrations of dissolved sulfide and dissolved iron, respectively (moles cm^{-3})

K = Solubility product, expressed with respect to those species for reservoir concentrations are defined.

and the maximum of j occurs at the distance $R_{j_{max}}$

$$R_{j_{max}} = \frac{a(D_S C_S^o + D_F C_F^o)}{D_F C_F^o}$$

These equations allow the rate of precipitation to be calculated, for a steady state, at any point between the two reservoirs. Values of D_S and D_F are taken for seawater from Boudreau and Canfield (1988) as 376 and 149 cm^{-2} yr^{-1} respectively. In the model calculations (fig. 3) a typical porewater pH of 7.5 is assumed, and the concentrations of dissolved sulfide and dissolved iron have been chosen by reference to porewaters in analogous carbon-rich modern sediments (Canfield and Raiswell, 1991a).

References

Aller, R. C., and Yingst, J. Y., 1978, Biogeochemistry of tube dwellings: a study of the sedentary polychaete *Amphitrite ornata (Leids):* Journal of Marine Research, v. 36, p. 201–254.

Alperin, M. J., ms, 1989, The carbon cycle in an anoxic marine sediment: concentrations, rates, isotope ratios and diagenetic models: Ph. D. thesis, University of Alaska, 241p.

Ben Yaakov, S., 1973, pH buffering of pore water of recent anoxic marine sediment: Limnology and Oceanography, v. 18, p. 86–94.

Berner, R. A., 1967, Thermodynamic stability of sedimentary iron sulfides: American Journal of Science, v. 265, p. 773–785.

———— 1970, Sedimentary pyrite formation: American Journal of Science, v. 268, p. 1–23.

Berner, R. A., Scott, M. R., and Thomlinson, C., 1970, Carbonate alkalinity in the pore waters of anoxic marine sediments: Limnology and Oceanography, v. 15, p. 544–549.

Berner, R. A., Westrich, J. T., Graber, R., Smith, J., and Martens, C., 1978, Inhibition of aragonite precipitation for supersaturated sea-water: A laboratory and field study: American Journal of Science, v. 278, p. 816–837.

Blatt, H., and Brown, V. M., 1974, Prophylactic separation of heavy minerals: Journal of Sedimentary Petrology, v. 44, p. 260–261.

Boudreau, B. P., and Canfield, D. E., 1988, A provisional diagenetic model for pH in anoxic porewaters. Journal of Marine Research, v. 46, p. 429–455.

———— 1993, A comparison of closed and open system models for porewater pH and calcite saturation state: Geochimica et Cosmochimica Acta, v. 57, p. 317–334.

Canfield, D. E., 1989, Reactive iron in marine sediments: Geochimica et Cosmochimica Acta, v. 53, p. 619–632.

Canfield, D. E. and Des Marais, D. J., 1992, Aerobic sulfate reduction in microbial mats: Science, v. 251, p. 1471–1473.

Canfield, D. E., and Raiswell, Rob, 1991a, Pyrite formation and fossil preservation, *in* Allison, P. A., and Briggs, D. E. G., editors, Taphonomy: releasing the data locked in the fossil record: New York, Plenum Press, p. 337–387.

———— 1991b, Precipitation and dissolution of carbonates: implications for fossil preservation, in Allison, P. A., and Briggs, D. E. G., editors, Taphonomy: releasing the data locked in the fossil record: New York, Plenum Press, p. 411–453.

Carstens, H., 1986, Displacive growth of authigenic pyrite: Journal of Sedimentary Petrology, v. 56, p. 252–257.

Chambers, L. A., and Trudinger, P. A., 1978, Microbiological fractionation of stable sulfur isotopes: a review and critique: Journal of Geomicrobiology, v. 1, p. 249–293.

Claypool, G. E., Holser, W. T., Kaplan, I. R. Sakai, I. I., and Zak, I., 1980, The age curves of sulfur and oxygen isotopes in marine sulfate and their mutual interpretation: Chemical Geology, v. 28, p. 199–260.

Coleman, M. L., 1985, Geochemistry of diagenetic non-silicate minerals: kinetic considerations: Philosophical Transactions of the Royal Society of London, v. 315A, p. 39–56.

Coleman, M. L., Curtis, C. D., and Irwin, II., 1979, Burial rate a key to source and reservoir potential: World Oil, v. 188, p. 83–92.

Coleman, M. L., and Raiswell, Rob, 1981, Carbon, oxygen and sulphur isotope variations in concretions from the Upper Lias of N.E. England: Geochimica et Cosmochimica Acta, v. 45, p. 329–340.

———— 1993, Microbial mineralization of organic matter: mechanisms of self-organmization and inferred rates of precipitation of diagenetic minerals. Philosophical Transactions of the Royal Society of London, v. A344, p. 69–87.

Curtis, C. D., 1977, Sedimentary geochemistry: environments and processes dominated by involvement of an aqueous phase: Philosophical Transactions of the Royal Society of London, v. 286A, p. 353–372.

Curtis, C. D., Coleman, M. L., and Love, L. G., 1986, Pore water evolution during sediment burial from isotopic and mineral chemistry of calcite, dolomite and siderite concretions: Geochimica et Cosmochimica Acta, v. 50, p. 2321–2334.

Devol, A. II and Ahmed, S. I., 1983, Are higher rates of sulphate reduction associated with anaerobic methane oxidation?: Nature, v. 291, p. 407–408.

Drobner, E., Huber, H., Wächtershäuser, G., Rose, D., and Stetter, K. O., 1990, Pyrite formation linked with hydrogen evolution under anaerobic conditions: Nature, v. 346, p. 742–744.

Goldhaber, M. B., and Kaplan, I. R., 1974, The sulfur cycle, *in* Goldberg, E. D., editor, The Sea, v. 5: New York, John Wiley and Sons, p. 569–655.

———— 1980, Mechanisms of sulfur incorporation and isotope fractionation during early diagenesis in sediments of The Gulf of California: Marine Chemistry, v. 9, p. 95–143.

Gautier, D. L., 1982, Siderite concretions—indications of early diagenesis in the Gammon Shale (Cretaceous): Journal of Sedimentary Petrology, v. 52, p. 859–871.

Helfferich, F., and Katchalsky, A., 1970, A simple model of interdiffusion with precipitation: Journal of Physical Chemistry, v. 74, p. 231–240.

Howarth, M. K., 1962, The Jet Rock Series and the Alum Shale Series of the Yorkshire Coast: Proceedings of the Yorkshire Geological Society, v. 33, p. 381–422.

Irwin, H., Curtis, C. D., and Coleman, M., 1977, Isotopic evidence for source of diagenetic carbonates formed during the burial of organic-rich sediments: Nature, v. 269, p. 209–213.

Jørgensen, B. B., and Revsbech, N. P., 1983, Colorless sulfur bacteria, Beggiatoa spp. and Thiovulum spp., in O2 and H2S microgradients: Applied Environmental Microbiology, v. 45, p. 1261–1270.

Kharaka, Y. K., Gunter, W. D., Aggarwall, P. K., Perkins, E. H., and deBrall, J. D., Solmineq.88: A computer program code for geochemical modeling of water-rock interactions: United States Geological Survey Water Investigations Report 88.

Lovley, D. R., Chapelle, F. II, and Phillips, E. J. P., 1990, Fe(III)-reducing bacteria in deeply buried sediments of the Atlantic Coastal Plain: Geology, v. 18, p. 954–957.

Mast, R. F. & Potter, P. E., 1963, Sedimentary structures, Sand-shape fabrics, and permeability, Part II: Journal of Geology, v. 71, p. 548–565.

Maxwell, J. A., 1968, Rock and Mineral Analysis: New York, Wiley-Interscience, 58 p.

O'Brien, N. R., 1990, Significance of lamination in Toarcian (Lower Jurassic) shales from Yorkshire, Great Britain: Sedimentary Geology, v. 67, p. 25–34.

Pettijohn, F. J., Potter, P. E., and Siever, R., 1973, Sand and sandstone: New York. Springer-Verlag, p. 524–533.

Pisciotto, K. A. and Mahoney, J. J., 1981, Isotopic survey of diagenetic carbonates, Deep Sea Drilling Project: Initial Reports of the Deep Sea Drilling Project, v. 63, p. 595–609.

Raiswell, Rob, 1971, The growth of Cambrian and Liassic carbonate concretions: Sedimentology, v. 17, p. 227–241.

———— 1976, The microbiological formation of carbonate concretions in the Upper Lias of N.E. England: Chemical Geology, v. 18, p. 227–244.

———— 1978, Non-steady state microbiological diagenesis and the origin concretions and nodular limestone, *in* Marshall, J. D., editor, Geological Society of London Special Publication, v. 36: Oxford, Blackwell Scientific, p. 41–54.

———— 1982, Pyrite texture, isotopic composition and the availability of iron, American Journal of Science, v. 282, p. 1244–1263.

———— 1988, Evidence for the surface-reaction controlled growth of carbonate concretions in shales: Sedimentology, v. 35, p. 571–575.

Raiswell, Rob, Buckley, F., Berner, R. A., and Anderson, T. F., 1988, Degree of pyritisation of iron as a paleoenvironment indicator of bottom water oxygenation: Journal of Sedimentary Petrology, v. 58, p. 812–819.

Raiswell, Rob, Whaler, K., Dean, S., Coleman, M. L., and Briggs, D. E. G., 1993, A simple three dimensional model of diffusion plus precipitation applied to localised pyrite formation in framboids, fossils and detrital iron minerals: Marine Geology, v. 113, p. 89–100.

Raiswell, Rob, and White, N. J. M., 1978, Spatial aspects of concretionary growth in the Upper Lias of N.F. England: Sedimentary Geology, v. 20, p. 291–300.

Reeburgh, W. S., 1983, Rates of biogeochemical processes in anoxic sediments: Annual Reviews of Earth and Planetary Science Letters, v. 11, p. 269–298.

Sackett, W. M., and Thompson, R. R., 1963, Isotopic organic carbon compositions of Recent continental shelf derived sediments of Eastern Gulf Coast, Gulf of Mexico: Bulletin of the American Association of Petroleum Geologists, v. 47, p. 525–531.

Schoonen, M. A. A., and Barnes, H. L., 1991, Reactions forming pyrite and marcasite from solution I. Nucleation of FeS_2 below 100°: Geochimica et Cosmochimica Acta, v. 55, p. 1495–1504.

Schwarcz,, H. P., 1969, Carbon, *in* Wedepohl, K. H., editor, Handbook of Geochemistry: Chapter 6B: Berlin Springer-Verlag, p. 6–8.

Sweeney, R. E., and Kaplan, I. R., 1973, Pyrite framboid formation: laboratory synthesis and marine sediments: Economic Geology, v. 68, p. 618–634.

Westrich, J. T., ms, 1983, The consequences and controls of bacterial sulfate reduction in marine sediments, Ph.D thesis, Yale University.